Contrib Mineral Petrol (1989) 102:257–264

Contributions to Mineralogy and Petrology

The system tonalite-peridotite-H_2O at 30 kbar, with applications to hybridization in subduction zone magmatism

A. Dana Johnston[1] **and Peter J. Wyllie**[2]

[1] Department of Geological Sciences, University of Oregon, Eugene, OR 97403-1272, USA
[2] Division of Geological and Planetary Sciences, California Institute of Technology, Pasadena, CA 91125, USA

Abstract. We present data on the phase relationships of mixtures between natural tonalite and peridotite compositions with excess H_2O at 30 kbar, and on the composition of the piercing point where the peridotite-tonalite mixing line intersects the L(Ga,Opx) reaction boundary. These data, in conjunction with earlier analogous data along peridotite-granite and basalt-granite mixing lines, permit construction of a pseudoternary liquidus projection that is relevant to interaction of peridotite with slab-derived magmas. Knowledge of the liquidus phase and temperature for a range of compositions within this projection enables us to map primary crystallization fields for quartz, garnet, orthopyroxene, clinopyroxene, and olivine, and to estimate the distribution of isotherms across the projection. Using this projection, we explore the consequences of peridotite assimilation by mafic to intermediate (basalt to dacite) hydrous slab-derived melts. Progressive assimilation under isothermal conditions results in garnet precipitation as the melt composition traverses the garnet liquidus surface and then garnet + orthopyroxene crystallization once the melt reaches the L(Ga,Opx) field boundary. The melt is constrained to remain on this field boundary and further assimilation of peridotite simply results in continued precipitation of garnet + orthopyroxene until the melt is consumed. The product is a hybrid solid assemblage consisting of Ga + Opx. It is noteworthy that this process drives the melt composition in a direction nearly perpendicular to the mixing line between peridotite and the initial melt. If assimilation occurs with increasing temperature (as might occur if a slab-derived magma rises into the hotter mantle wedge), intermediate magmas (e.g. andesites) will again precipitate garnet until they reach the L(Ga,Opx) reaction boundary at which point Ga re-dissolves and orthopyroxene precipitates as the melt composition moves up-temperature along this boundary. The product of this process is a hybrid solid assemblage with garnet subordinate to orthopyroxene. For more mafic initial compositions (e.g. basalts) originally plotting in the Cpx field, it appears possible to avoid field boundaries involving garnet and shift in composition more directly toward peridotite, if assimilation is accompanied by a sharp increase in temperature. Considering published REE evidence (arguing against garnet playing a significant role in the genesis of many subduction-related magmas) in light of our results, it appears unlikely that peridotite assimilation by intermediate magmas under conditions of constant or increasing temperature is an important process in subduction zones. However, if assimilation is accompanied by an increase in temperature, our data do permit the derivation of high-Mg basalts from less refractory precursors (e.g. high-Al basalts) by peridotite assimilation.

Offprint requests to: A.D. Johnston

Introduction

Hildreth et al. (1986), in their introduction to the proceedings of a symposium on "Open Magmatic Systems", referred to the "mounting evidence that mixing and assimilation are ubiquitous, and that heterogeneity and mixing in mantle source regions are common". With respect to andesite genesis, "the complexity of most new models and their inadequacy in explaining all of the available evidence indicate that we are still far from a complete understanding."

Nicholls and Ringwood (1973) originally proposed that assimilation of mantle peridotite by an ascending slab-derived melt might be an important process in the generation of island arc volcanic rocks. They suggested that the melts would react with overlying peridotite forming zones of hybrid olivine pyroxenite which, in turn, could be remelted to generate a spectrum of island arc magmas. More recently, interaction of slab-derived melts with mantle peridotite has been invoked to account for the isotopic and trace element systematics of some arc volcanics (e.g. Myers 1988). Mixing processes in the mantle near convergent plate boundaries are also suggested by the conclusion of Volpe et al. (1987) from geochemical evidence that Mariana Trough basalts were formed by mixing at or near the source region in the mantle of MORB-like melt with an arc-like melt. Keleman and Ghiorso (1986) and Keleman (1986) have thoroughly examined the problem at low pressure by theoretical modeling.

In this contribution we present the results of additional experimental studies designed to investigate the products of reaction between hydrous melts derived from subducted oceanic crust, and the overlying mantle wedge.

Previous experimental approaches

The overall objective of this experimental program is to better understand the phase equilibrium controls on hybridization of rocks and melts that might be juxtaposed at depth in a convergent plate boundary region.

One way to investigate the products of hybridization is to

examine phase relations in synthetic silicate systems. Sekine and Wyllie (1982a, 1982b) explored published data in systems containing representatives of hydrous siliceous magmas and mantle peridotite, and demonstrated that hybridization is not a simple mixing process, because of the incongruent melting of enstatite and phlogopite. In another approach, Sekine and Wyllie (1982c) used whole rock powders as starting materials, and showed that the phase fields intersected by peridodite-granite-H_2O at 30 kbar are directly analogous to those in the model synthetic systems. In a third approach, Sekine and Wyllie (1983) performed experiments with hydrous granitic liquid in contact with solid peridotite. The solubility of peridotite components in the granite liquid under these conditions is low, as anticipated from the synthetic systems, and the change in composition of the liquid is constrained by liquidus field boundaries between the two components. The hybrid crystalline product of the reaction is a zone of garnet pyroxenite, with the role of phlogopite still undefined.

Our principal objective is to present new results which, in conjunction with the results cited above and those of Stern and Wyllie (1978), place reasonably tight constraints on the form of a liquidus phase diagram that is relevant to interaction of peridotite with melts derived by partial fusion of subducted oceanic crust. The utility of such liquidus phase diagrams for complex rock systems is well-known. Using these diagrams, it is a relatively straightforward matter to determine if two melts are related through fractionation along an equilibrium liquid line of descent or if more complex processes such as magma mixing, wall-rock assimilation or periodic replenishment of a magma chamber with fresh magma must be invoked to relate them. Furthermore, liquidus phase diagrams provide the ability to predict the consequences of a wide variety of processes such as those mentioned above.

Liquidus phase diagrams for complex natural systems are now quite well-known at 1 atmosphere pressure and have been utilized to good advantage by many authors concerned with the origin and evolution of MORB (e.g. Walker et al. 1979; Grove and Bryan 1983) and calc-alkaline series rocks (e.g. Baker and Eggler 1983; Grove et al. 1982; Grove and Baker 1984). Our knowledge of the liquidus diagram at higher pressures, however, is much less complete (e.g. Stolper 1980; Baker and Eggler 1987; Takahashi and Kushiro 1983).

There are at least two means by which liquidus phase fields and boundaries may be determined in compositionally complex rock systems. One approach is to analyze large numbers of multiply saturated experimental glasses. These compositions are then plotted in appropriate projections where they define the various cotectic and reaction boundaries corresponding to the crystalline phase assemblages with which the melts were in equilibrium.

An alternative approach, and that used here, is to determine the liquidus mineral and temperature of a series of compositions produced by mixing two endmember natural rock powders in various proportions. If two compositions along such a mixing line have different minerals on their liquidii, it may be concluded that the cotectic or reaction boundary involving these two minerals lies between the two compositions. Our goal is to locate such piercing points, where various mixing lines through composition space intersect the phase boundaries of interest.

The results cited above, along with those of earlier experiments, have been compiled in Fig. 1 to provide a working framework for this 30 kbar study of compositions ranging from tonalite to peridotite. The lines separating the fields for crystallization of the minerals shown are based on the results of Stern and Wyllie (1978) for the join basalt-granite (B-G) and Sekine and Wyllie (1982c) for the join peridotite-granite (P-G). Stern and Wyllie (1978) emphasized that these lines are not ternary phase boundaries, but the intersections of crystallization surfaces in multicomponent space with the composition surface containing the projected compositions of the rocks considered. It has been established, however, that the projected positions of liquid paths followed by crystallizing liquids in some of the rock compositions do approximate fairly closely some of the boundaries (Stern and Wyllie 1978; Carroll and Wyllie 1989). Because Al_2O_3 and the alkalies are not represented in this projection, caution must be exercised when applying Fig. 1 to compositions differing significantly from basalt, tonalite, granite, peridotite and linear combinations of these rock compositions.

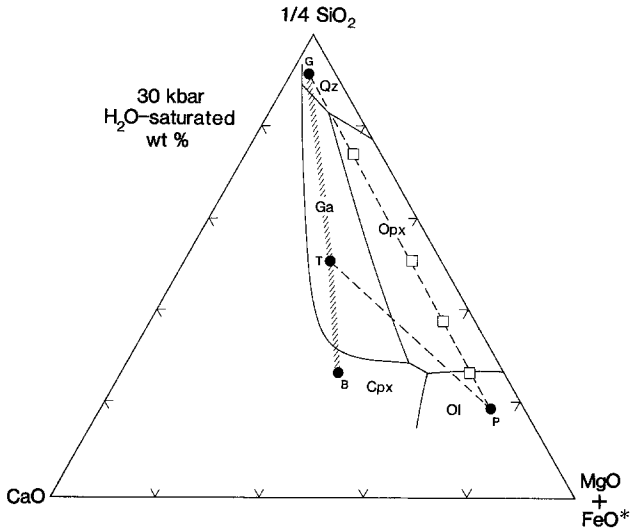

Fig. 1. H_2O-saturated pseudoternary liquidus phase relations at 30 kbar projected onto the plane $1/4SiO_2 - CaO - (FeO^* + MgO)$. Estimated by Sekine and Wyllie (1982c) from their results (*open squares*) along the join granite (*G*)-peridotite (*P*) and from the results of Stern and Wyllie (1978) along the join basalt (*B*)-G. Experiments reported here utilized mixtures along the join P – Tonalite (*T*) (see Fig. 2). The *diagonally-ruled line* (*G*–*B*) represents the average natural calc-alkaline trend. Primary crystallization fields are shown for quartz (*Qz*), garnet (*Ga*), orthopyroxene (*Opx*), olivine (*Ol*), and clinopyroxene (*Cpx*)

To provide the complete physico-chemical framework within which the origin and evolution of magmatic liquids may be interpreted, multi-dimensional composition space must be investigated at liquidus temperatures over a wide range of pressures, water contents, oxygen fugacities etc. Eventually it may be possible to compute the liquidus paths and their variation with these variables (e.g. Ghiorso 1987; Ghiorso and Carmichael 1987), but in the meantime our aim here is to add another constraint, by study of the composition join peridotite-tonalite (P-T, Fig. 1). This join intersects the as yet undetermined boundary between the fields for primary crystallization of garnet and orthopyroxene which appears to be the main control on reactions between eclogite-derived hydrous melts and peridotite.

Starting materials

Starting materials consisted of finely ground natural tonalite from the Central Sierra Nevada Batholith (#101 of Piwinskii 1968a), and partially hydrated peridotite mylonite from St. Paul's Rocks (#18-900) kindly supplied by W.G. Melson. Detailed accounts of the mineralogy and petrology of the tonalite were given by Piwinskii (1968b) and of the peridotite by Melson et al. (1967, 1972) and Frey (1970). Major element chemical analyses of both samples are listed in Table 1. Hydrous phase relations at 30 kbar have been reported for the tonalite by Stern and Wyllie (1978) and for the peridotite by Millhollen et al. (1974), Nehru and Wyllie (1975), and Sekine and Wyllie (1982c).

The compositions of four mixtures prepared from the crystalline tonalite (T) and peridotite (P) are listed in Table 1 and plotted in Fig. 2 as M1 (90T10P), M2 (80T20P), M3 (70T30P), and M4 (60T40P). These mixtures contain 1.33, 1.80, 2.29, and 2.78 wt% H_2O respectively. Known weights of additional water were added to the mixtures in gold capsules, and Table 2 lists these values

Table 1. Chemical compositions of starting materials

	1	2	M1	M2	M3	M4
SiO_2	59.14	42.22	57.36	55.76	54.08	52.86
TiO_2	0.79	0.30	0.74	0.69	0.64	0.59
Al_2O_3	18.23	4.42	16.78	15.47	14.10	12.72
Cr_2O_3	–	0.50	0.05	0.10	0.15	0.20
Fe_2O_3	2.32	2.86	2.38	2.43	2.48	2.53
FeO	3.62	4.45	3.71	3.79	3.87	3.95
MnO	0.11	0.13	0.11	0.11	0.12	0.12
NiO	–	0.27	0.03	0.05	0.08	0.11
MgO	2.50	34.61	5.87	8.92	12.10	15.31
CaO	5.92	3.92	5.71	5.52	5.32	5.12
Na_2O	3.81	0.43	3.45	3.13	2.80	2.46
K_2O	2.19	0.11	1.97	1.77	1.57	1.36
H_2O^+	0.82	5.73	1.33	1.80	2.29	2.78
H_2O^-	0.04	0.19	0.06	0.07	0.08	0.10
P_2O_5	0.30	0.05	0.27	0.25	0.22	0.20
Cl	–	0.20	0.02	0.04	0.06	0.08
CO_2	0.01	–	0.01	0.01	0.01	0.01
Total	99.80	100.39	99.85	99.91	99.97	100.50
Mg#[a]	43.9	89.8	64.1	72.7	77.9	81.4

[a] Mg# = 100(Mg/(Mg+Fe))

1. Tonalite (101); Bateman et al. (1963)
2. St. Paul's peridotite mylonite; Melson et al. (1967, 1972)
M1. Mixture of 89.5% Number 1 and 10.5% Number 2
M2. Mixture of 80.0% Number 1 and 20.0% Number 2
M3. Mixture of 70.1% Number 1 and 29.9% Number 2
M4. Mixture of 60.1% Number 2 and 39.9% Number 2

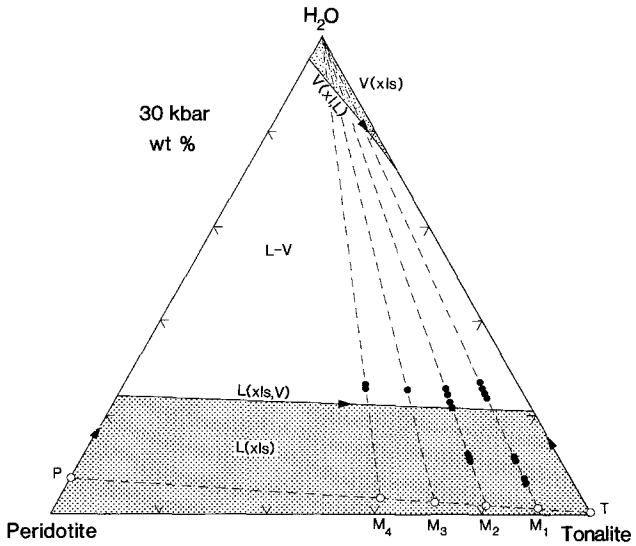

Fig. 2. Experimental mixtures projected onto the plane peridotite-tonalite-H_2O. *Open circles* labelled *M1–M4* represent the starting mixtures (see Table 1) and contain water primarily bound in minerals in the hydrated peridotite endmember. *Filled circles* represent the actual compositions of the experimental charges which contained additional water. The *shaded areas* are the estimated H_2O-undersaturated liquidus surface, and the subsolidus vaporus surface (after Sekine and Wyllie 1982c). Abbreviations: *xls*: crystals; *L*: liquid; *V*: vapor

together with the total water present in each run. The compositions of all runs are plotted in Fig. 2.

As a framework for selection and interpretation of runs, Fig. 2 also shows the estimated positions of the field boundaries for the H_2O-saturated liquidus, and for the coexisting vaporus boundary.

Table 2. Experimental results at 30 kbar

Run	Mixture	%H_2O added	%H_2O[a] total	T (°C)	Duration (hours)	Assemblage
75	M1	26.5	27.5	1050	16.5	L, V
93	M1	24.7	25.7	1025	17.5	Ga,L,V
77	M1	23.4	24.4	950	70.0	Ga,L,V
76	M1	25.3	26.4	900	43.0	Ga,Cpx,L,V
79	M1	10.6	11.8	1100	25.0	Ga,L
78	M1	10.8	12.0	1050	24.0	Ga,Cpx,L
81	M1	6.3	7.6	1170	22.0	Ga,L
80	M1	5.3	6.5	1170	24.0	Ga,L
87	M2	21.3	22.7	1150	21.0	L, V
89	M2	21.4	22.7	1100	25.0	L, V
90	M2	24.8	26.2	1075	20.0	L, V
91	M2	23.7	25.1	1062	23.0	Ga,L,V
86	M2	22.3	23.7	1050	22.5	Ga,Opx,L,V
85	M2	11.0	12.6	1150	20.5	Ga,Opx,L
83	M2	9.9	11.5	1100	25.0	Ga,Opx,L
82	M2	10.2	11.9	1050	29.0	Ga,Opx, Cpx(?),L
99	M3	24.5	26.2	1125	4.0	Opx,L,V
97	M4	25.0	27.1	1150	23.5	Opx,L,V
95	M4	24.8	26.9	1125	18.5	Opx,L,V

[a] Equals water added plus that present in starting materials

Ga: garnet; *Opx*: orthopyroxene; *Cpx*: clinopyroxene; *L*: liquid; *V*: vapor

Most of our charges contained sufficient H_2O to saturate the liquid.

Experimental and analytical methods

High pressure experiments

Experiments were performed in a single-stage piston-cylinder apparatus similar to that described by Boyd and England (1960), using a 0.5 inch-diameter chamber and piston. The apparatus was calibrated for pressure and temperature as described by Boettcher and Wyllie (1968). Temperatures, measured with W5Re/W26Re thermocouples, were controlled to within ±5° C of the set point by a digital, solid state controller manufactured by Eurotherm Corp., and were accurate to ±15° C. No correction was applied for the effect of pressure on thermocouple EMF. Furnace assemblies consisted of an outer cylinder of NaCl containing the high purity graphite furnace tube which in turn contained an upper hollow NaCl cylinder, through which the thermocouple passed, and a lower solid NaCl pedestal containing the capsule (see below). All runs were brought to final pressure (30 kbar) with the "hot piston-out" procedure as described by Boyd et al. (1967). Pressures listed in Table 2 are nominal, incorporate no corrections for friction and are considered accurate to ±5%. Oxygen fugacity was not buffered but Fe-Ti oxide equilibration runs utilizing the same furnace assembly yield fO_2's near the synthetic Ni-NiO buffer curve (Carroll and Wyllie 1989).

Gold capsules were used in all experiments to minimize the effects of Fe-loss to the capsule. After loading the dry rock powder and water, the capsule was sealed by arc-welding and then loaded into a die with powdered NaCl and pressed into the solid pedestal that fit in the bottom of the furnace tube. In this way all empty space around the capsule was eliminated. The capsule was near the top of the pedestal and care was taken to ensure that no more than 1 mm of NaCl was present between the capsule and the thermocouple tip. After each run, the NaCl pedestal was dissolved

in warm water and the capsule was dried and weighed to check for leakage.

Experiments were run for 4 h–70 h. At the end of each run, the sample was quenched by turning off the power to the furnace. The melt quenched to an intimate mixture of glass containing bubbles, and a mixed-layer smectite-type clay containing small (~4–20 μm), usually euhedral crystals of the equilibrium mineral(s). A portion of these powders was mounted for examination by conventional optical methods, and another portion was mixed in epoxy and polished until crystals appeared at the surface which could be analyzed by electron microprobe.

Analytical methods

Electron microprobe analyses were performed on the automated JEOL microprobe at the University of Washington. The analyses were performed using a sample current of 5 nA and an accelerating potential of 15 kV. Standards consisted of a variety of natural minerals, synthetic oxides and pure metals. Data reduction was performed on-line using the procedure of Bence and Albee (1968).

Experimental results

The results of our experiments are summarized in Table 2. All experiments were performed at 30 kbar and most contained sufficient H_2O (>21 wt%) to oversaturate the melt. The phase fields intersected by mixtures with excess water are shown in Fig. 3. All charges that contain bubbles are interpreted to be the products of vapor present conditions during the runs. When possible, the liquidus temperature was bracketed by runs 25° C apart (mixtures M1 and M2). For mixtures M3 and M4, however, the liquidus was at a temperature higher than the melting point of the gold capsules at 30 kbar. Because only one crystalline phase was present in the highest temperature runs with M3 and M4, the liquidus phase was identified despite the fact that the liquidus temperature could not be bracketed. The liquidus temperatures for M3 and M4 were estimated by extrapolating the decreasing abundance of crystals from the lowest temperature runs through runs at successively higher temperatures. The data for the tonalite end-member shown on Fig. 3 are from Stern and Wyllie (1978, Fig. 2b).

The liquidus phase for mixtures M1 and M2 is garnet, whereas that for mixtures M3 and M4 is orthopyroxene (Fig. 3). These results show that the phase boundary L(Ga,Opx) must lie between mixtures M2 and M3. Moreover, the absence of a thermal minimum at this boundary (Fig. 3) demonstrates that it is a reaction boundary and not a cotectic. The sub-liquidus phase relations have been estimated in Fig. 3 but we note that they become increasingly uncertain as the proportion of peridotite in the mixture increases and the temperature decreases.

Unfortunately we do not have enough runs from the H_2O-undersaturated region to construct sections similar to Fig. 3 at lower water contents. However, the five runs with ~11–12 wt% H_2O (Table 2) together with Stern and Wyllie's (1978) results with lower H_2O contents suggest that the topology of the phase boundaries remains similar to that with excess water, but that the boundaries move to higher temperatures as would be expected.

Analytical results

Representative electron microprobe analyses of liquidus and near-liquidus garnet and orthopyroxene crystals produced in runs with mixtures M1, M2, and M3 are given in Table 3. Although attempts were made, satisfactory broad-beam analyses of the quenched "glass" could not be obtained, nor could analyses of the tiny crystals be obtained in some of the charges. However, unequivocal identifications of the crystalline phases could be made in most instances.

The garnet analyses are pure pyrope-grossular-almandine solid solutions and range in composition from $Py_{61}Gr_{13}Alm_{26}$ to $Py_{71}Gr_{10}Alm_{19}$, with the more pyrope-rich compositions occurring in the more peridotite-rich mixtures. The orthopyroxene analyses display only a limited range in composition (En_{89-91}) and have relatively low abundances of Al_2O_3 (2–3 wt%). Averages of the analyses in Table 3 have been plotted in the projection shown in Fig. 5.

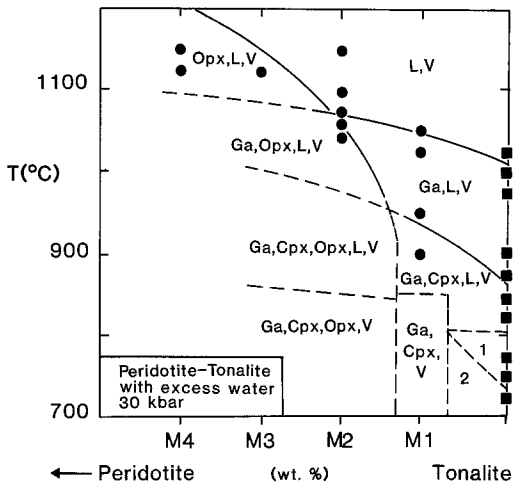

Fig. 3. Estimated H_2O-saturated phase relations at 30 kbar in the system peridotite-tonalite-H_2O. The results for the tonalite end-member (*squares*) are from Stern and Wyllie (1978); all other run points are from this study. The phase assemblages for fields labelled *1* and *2* are Ga+Cpx+Qz+L+V and Ga+Cpx+Qz+V, respectively

Table 3. Mineral compositions from selected runs at 30 kbar

Phase	Garnet		Orthopyroxene	
Mixture[a]	M1	M2	M2	M3
wt% H_2O[b]	25.7	23.7	23.7	26.2
T (°C)	1025	1050	1050	1125
Run #	93	86	86	99
SiO_2	41.27	41.99	54.43	55.15
TiO_2	0.08	0.06	0.00	0.03
Al_2O_3	21.94	22.21	2.57	2.90
FeO[c]	12.74	9.35	7.26	5.47
MnO	0.44	0.31	0.10	0.14
MgO	16.86	20.29	32.02	32.78
CaO	5.10	3.93	0.54	0.54
Na_2O	0.03	0.05	0.05	0.04
K_2O	0.03	0.09	0.00	0.05
Total	98.49	98.28	96.97	97.08

[a] Same abbreviations as Table 1
[b] wt% H_2O added plus that in the starting materials
[c] Total Fe reported as FeO

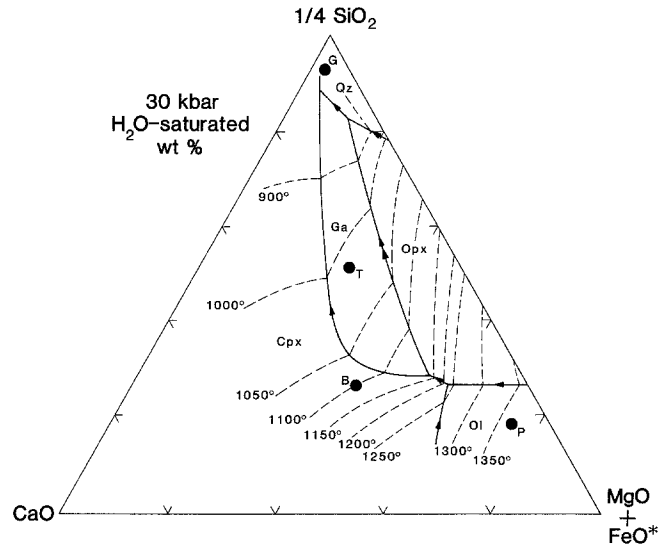

Fig. 4. H_2O-saturated liquidus phase relations at 30 kbar projected onto the plane $1/4SiO_2 - CaO - (FeO^* + MgO)$. Isotherms have been estimated from the results of Stern and Wyllie (1978) along the join B–G, Sekine and Wyllie (1982) along the join P–G, and this study along the join T – P. Abbreviations: same as in Fig. 1

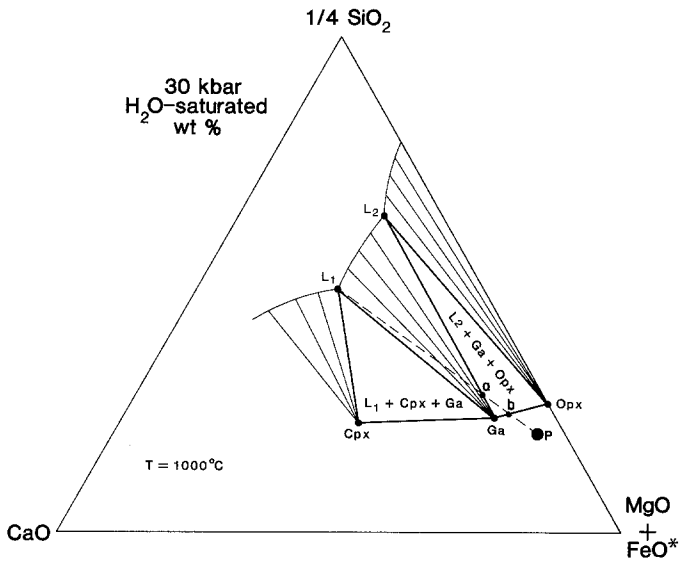

Fig. 5. Pseudoternary isothermal isobaric section at 1000° C, illustrating the effect of peridotite assimilation by a slab-derived tonalitic melt under conditions of constant temperature. As peridotite (*P*) is added to an initial melt (L_1) on the L(*Ga,Cpx*) field boundary, the bulk composition traverses the garnet liquidus surface resulting in garnet crystallization and driving the residual melt to L_2, corresponding to the intersection of the 1000° C isotherm with the L(Ga,Opx) field boundary. The melt composition is constrained to remain at this point where, with further addition of peridotite, garnet and orthopyroxene crystallize together until the remaining melt is consumed at point *b*. Note that assimilation of peridotite by hydrous tonalitic melt under isothermal conditions drives the liquid composition along a path that is nearly orthogonal to the mixing line L_1–P. The points labeled Ga and Opx are averages of the experimentally determined compositions in Table 3

Liquidus phase diagram at 30 kbar

In Fig. 4 we have combined the results presented above on peridotite-tonalite mixtures with the earlier results of Sekine and Wyllie (1982c) and present them in the $1/4SiO_2$–CaO–(FeO* + MgO) projection discussed earlier. In Fig. 1, the field boundary L(Cpx,Ga) and the piercing point where the basalt-granite mixing line crosses L(Ga,Qz) are from Stern and Wyllie (1978), and the piercing point where the peridotite-granite mixing line crosses L(Qz,Opx) is from Sekine and Wyllie (1982c). The new results in Fig. 3 for the piercing point where the tonalite-peridotite mixing line crosses L(Ga,Opx) provide one fix on the position of this field boundary in Fig. 4. This boundary is further constrained to lie to the right of the basalt-granite mixing line and between the two piercing points taken from Stern and Wyllie (1978) and Sekine and Wyllie (1982c) discussed above. The field boundary L(Ga,Opx) is a reaction boundary along which orthopyroxene dissolves and garnet precipitates with decreasing temperature.

The piercing points and field boundaries outline the fields for primary crystallization of olivine, clinopyroxene, orthopyroxene, garnet, and quartz. The results for the liquidus profiles on the joins in Fig. 1 (B-G, Stern and Wyllie 1978; P–G, Sekine and Wyllie 1982c; and P-T, this work) permit us to sketch, isotherms across the projected H_2O-saturated liquidus surface, with results as shown in Fig. 4.

Isobaric isothermal section

From the liquidus diagram in Fig. 4, we obtain the liquidus isotherm for 1000° C in Fig. 5, with L_1 and L_2 representing liquid compositions on the field boundaries L(Ga,Cpx) and L(Ga,Opx), respectively. The projected compositions of orthopyroxene and garnet coexisting with liquid have been taken from Table 3 and the clinopyroxene composition was estimated from Stern and Wyllie (1978). These data permit construction of the pseudoternary isothermal isobaric section shown in Fig. 5. Despite the fact that the compositions of liquid and all minerals have been projected onto this triangular diagram, the phase assemblages involved are simple enough that the treatment of the triangle as if it were a ternary system should define reasonably well (in projection) the behavior of melts.

Consider mixing of liquid L_1 and crystalline peridotite P at 30 kbar at 1000° C with excess H_2O (Fig. 5). Addition of peridotite to L_1 at constant pressure and temperature shifts the bulk composition along the mixing line L_1–P, and into the 3-phase field for Ga + L + V. As a consequence, the peridotite phases dissolve and garnet is precipitated, and the liquid changes from L_1 towards L_2 along the 1000° C isotherm. With continued addition of peridotite the bulk composition reaches point *a* and the liquid composition reaches L_2, which corresponds to the intersection of the 1000° C isotherm with the L(Ga,Opx) field boundary in Fig. 4, where garnet is joined by the precipitation of orthopyroxene. The liquid is constrained to remain at this point, and further addition of solid peridotite results in the precipitation of garnet and orthopyroxene, until the bulk composition reaches point *b*, where the last melt crystallizes. The product is an assemblage consisting of garnet + orthopyroxene, in proportions given approximately (because of the pseudoternary nature of the diagram) by the position of point *b* on the join Ga-Opx.

Consider next the history of liquid L_1 reacting with the peridotite P under conditions where the temperature can increase as would occur if a slab-derived magma rose into the hotter overlying mantle wedge. The bulk composition changes along L_1–P as peridotite is dissolved. If the melt

is no longer constrained to follow an isotherm, the liquid composition will migrate across the garnet liquidus surface in Fig. 4, precipitating garnet and following a path displaced somewhat to the SiO_2 side of L_1–P but with obvious enrichment in peridotite components, until it reaches the field boundary L(Ga,Opx). At this reaction boundary, garnet will be resorbed and orthopyroxene will be precipitated as the liquid path changes direction and moves away from SiO_2 to travel in the up-temperature direction along the field boundary, which is oblique to the mixing line L_1–P.

In both of these examples, aqueous vapor is evolved continuously from the saturated liquid as crystals are precipitated. Dissolution of solid P in L_1 does change the composition of the liquid, *but not towards P.* The liquid paths are controlled by the phase relations, not by simple mixing of the two components. Only if the temperature of a liquid such as L_1 is raised sufficiently to elevate it above the liquidus surface can the liquid composition change directly toward the solid composition, P.

Petrological applications

Figures 1 and 4 show the positions of vapor-saturated field boundaries separating the liquidus fields for crystallization of primay olivine, clinopyroxene, orthopyroxene, garnet, and quartz at 30 kbar, equivalent to a depth of about 100 km, for bulk compositions including peridotite and the calc-alkaline rock series, with B also representing basalt of the oceanic crust. The field boundaries will change as a function of total pressure (e.g. see similar diagram at 15 kbar in Carroll and Wyllie 1989) but the changes may not be great through a fairly wide pressure interval, say 25–30 kbar (Wyllie 1979, Figs. 19–24). The temperature profiles and positions of the field boundaries will also vary as a function of water activity, but the boundaries associated with the garnet field experience their greatest changes from 0% to 5% H_2O, with much less change from 5% to saturation, as shown by Stern and Wyllie (1978, Figs. 4 and 15). Therefore the applications drawn from the H_2O-saturated phase diagrams in Figs. 1, 4, and 5 may also be relevant to rock systems with moderate water contents.

Magmas from subducted oceanic crust

Sekine and Wyllie (1982c) and Johnston (1986) concluded that the earliest melts generated by partial fusion of subducted oceanic crust at depths of about 100 km correspond to the highly siliceous compositions at the point of intersection of the liquidus fields for clinopyroxene, garnet, and quartz (coesite). Stern and Wyllie (1978) concluded that the compositions of liquids with progressive fusion would be controlled by the hyperdimensional equivalent of the boundary L(Cpx,Ga) in Figs. 1 and 4, and would therefore have higher CaO/(MgO + FeO) ratios than the average values in calc-alkaline rocks (Fig. 1). This conclusion was supported by the analogous experiments in the model system CaO–MgO–Al_2O_3–SiO_2–H_2O by Sekine et al. (1981).

Hybridization of hydrous magma rising from subducted slab into peridotite

The mixing reactions described above and by Sekine and Wyllie (1982c) illustrate the types of products that might be produced when a melt rises from subducted oceanic crust into the overlying mantle wedge. If the early siliceous melts are able to escape from the subducted slab and rise into the overlying mantle peridotite, the liquids assimilate peridotite with precipitation of phlogopite-garnet-pyroxenite, but with little change in the composition of the liquid. Liquid compositions remain in the vicinity of the L(Ga,Qz) field boundary until completely solidified (Sekine and Wyllie 1982c).

Consider a melt generated in hydrous oceanic crust composed of quartz eclogite. It will first dissolve quartz (coesite), then follow a polybaric field boundary corresponding to L(Ga,Cpx) in Fig. 4 as the temperature rises. If the melt escapes from the slab at 1000° C, its initial composition will be located at the intersection of the L(Ga,Cpx) field boundary and the 1000° C isotherm in Fig. 4. This melt will then rise to a region of lower pressure containing a higher temperature mass of peridotite with composition P. What happens to this melt as it assimilates peridotite depends on the balance between heat and mass transfer.

If assimilation occurs without much increase in temperature, the resulting melts will be depleted in CaO relative to the initial liquid and will have about the same ratio of SiO_2 to (FeO* + MgO). If temperature rises during the assimilation process, the resulting melts will be depleted in both CaO and SiO_2 and enriched in (FeO* + MgO) relative to the initial liquid. Also noteworthy is the fact that the crystalline phase assemblage in equilibrium with the melt after assimilation (Ga + Opx) will differ from that before assimilation (Ga + Cpx). The initial effect of hybridization of mantle peridotite and melts of intermediate SiO_2 content from subducted oceanic crust (melts on L(Ga,Cpx)) will be to increase the (MgO + FeO)/CaO ratio in the liquids, bringing them closer to the compositions of the average calc-alkaline series. There is nothing to limit their compositions to this series, however, and the liquids will tend to change composition until they are controlled by the field boundary L(Ga,Opx). These liquids have (MgO + FeO*)/CaO ratios considerably higher than those of average calc-alkaline compositions. Therefore, we suggest that the major element characteristics of the calc-alkaline magma series are not imposed by hydrous melting of subducted oceanic quartz eclogite, nor by hybridization of slab-derived melts with solid mantle peridotite at great depth (> 80 km).

Residual garnet and REE's

One of the often cited problems with a slab-source for arc volcanic rocks is that residual garnet in the quartz eclogite slab would produce steep chondrite-normalized rare earth element (REE) patterns with heavy REE depletion in the extracted melts, yet flat to slightly light REE-enriched REE patterns are ordinarily (but not always) observed (Gill 1974). From the discussion above, it is clear that interaction with peridotite is not an effective means to circumvent this problem because, in general, it will induce garnet crystallization. Johnston (1986) and Brophy and Marsh (1986) suggested instead that the degree of melting of the subducted slab might be sufficient to reduce or exhaust garnet in the source, leaving a residue consisting dominantly of clinopyroxene. It is of interest to follow the path of such a melt as it assimilates peridotite. Such a melt would plot to the left of the L(Ga,Cpx) field boundary in Fig. 4, in the field for primary crystallization of clinopyroxene (i.e. point *B* in Fig. 4). Figures 4 and 5 help to illustrate the path the

melt will follow as it assimilates peridotite (P). Isothermal assimilation of peridotite by the melt results in clinopyroxene precipitation (as the bulk composition traverses the Cpx liquidus surface), and drives the melt composition to the L(Ga,Cpx) field boundary, where garnet joins the crystallizing assemblage. Under isothermal conditions, the melt will be constrained to remain at this point, and further assimilation of peridotite simply causes further precipitation of garnet + clinopyroxene until the bulk composition reaches the Ga-Cpx join and the last melt is consumed.

In this scenario, assimilation of peridotite by basalt results in the reappearance of garnet in the residue from which it had earlier been removed by large degrees of partial melting. Such a mechanism could conceivably contribute to the relatively steep REE patterns displayed by some arc volcanics (e.g. Lopez-Escobar et al. 1977; Hildreth and Moorbath 1988), but conflicts with the near-flat REE patterns displayed by most arc volcanics. It is possible, however, that if assimilation occurs with increasing temperature, the liquid path could avoid the L(Ga,Cpx) field boundary altogether and the the final melt would lie along either the L(Cpx, Opx) or the L(Cpx,Ol) field boundaries (Fig. 4). Under these circumstances, with increasing temperature, it appears possible to enrich a slab-derived melt in peridotitic components through peridotite assimilation without inducing the appearance of garnet.

Assimilation, mixing and hybrid products

The examples outlined above confirm that mixing between melts and crystals does not normally involve simple linear mixing between the two endmembers (except in the case of superheated liquids which are considered to be petrologic rarities). Bowen's (1928) classic treatment of assimilation emphasized the fact that liquid compositions are constrained to follow field boundaries. The paths of contaminated magmas are controlled by thermal budgets and the shapes of liquidus surfaces and field boundaries. These may steer liquid compositions in directions almost orthogonal to the linear mixing lines between liquid and assimilated rock, as in the isothermal example of L_1 evolving to L_2 illustrated in Fig. 5.

Conclusions

1. The new experimental results together with earlier results permit construction of a H_2O-saturated projection at 30 kbar with fields for the primary crystallization of olivine, orthopyroxene, clinopyroxene, garnet, and quartz. Furthermore, knowledge of the liquidus temperatures of a range of compositions within the projection permits us to estimate the distribution of isotherms across these liquidus surfaces.
2. These results have been applied in an attempt to predict the consequences of peridotite assimilation by a slab-derived melt. In the case of nearly isothermal assimilation of peridotite, garnet precipitation results and the melt composition changes, but not toward peridotite. In fact, the melt composition follows a path that is nearly perpendicular to the mixing line between the original melt and peridotite. This, coupled with the REE evidence arguing against a significant role for garnet in the genesis of most subduction-related magmas suggests that nearly isothermal assimilation of peridotite may not ordinarily be an important process in subduction zones.
3. If the original melt is relatively basic (e.g. point *B*, Fig. 4) and assimilation is accompanied by a large temperature increase (as would occur when a slab-derived melt rises into the hotter mantle wedge), it is conceivable that the field boundaries involving garnet could be avoided and the melt could follow a path more directly toward peridotite. Thus, assimilation of peridotite under conditions of increasing temperature can conceivably produce high-Mg melts from lower-Mg melts as recently proposed by Myers (1988).
4. We suggest that neither hydrous melting of subducted oceanic quartz eclogite nor hybridization of slab derived melts controls the major element variations of the calc-alkaline magma series.

Acknowledgements. This research was supported by the Earth Sciences Section of the National Science Foundation, NSF Grants EAR-85-06857 (PJW) and EAR-88-16108 (ADJ). Reviews by Jim Brophy Jim Myers, Mike Naney and an anonymous reviewer are greatly appreciated. Alan Boudreau's assistance with the microprobe analyses is also gratefully acknowledged.

References

Baker DR, Eggler DH (1983) Fractionation paths of Atka (Aleutians) high-alumina basalts: constraints from phase relations. J Volcanol Geotherm Res 18:387–404

Baker DR, Eggler DH (1987) Compositions of anhydrous and hydrous melts coexisting with plagioclase, augite, and olivine or low-Ca pyroxene from 1 atm to 8 kbar: application to the Aleutian volcanic center of Atka. Am Mineral 72:12–28

Bateman PC, Clark L, Huber NK, Moore JG, Rhinehart CD (1963) The Sierra Nevada batholith, a synthesis of recent work across the central part. US Geol Surv Prof Pap 414-D, D1–D46

Bence AE, Albee AL (1968) Correction factors for electron probe microanalysis of silicates and oxides. J Geol 76:382–403

Boettcher AL, Wyllie PJ (1968) The quartz-coesite transition measured in the presence of silicate liquid and calibration of piston-cylinder apparatus. Contrib Mineral Petrol 17:224–232

Bowen NL (1928) The Evolution of the Igneous Rocks. Princeton University Press, Princeton, 332 pp

Boyd FR, England JL (1960) Apparatus for phase equilibrium measurements at pressures up to 50 kilobars and temperatures up to 1750° C. J Geophys Res 65:741–748

Boyd FR, Bell PM, England JL, Gilbert MC (1967) Pressure measurement in single-stage apparatus. Carnegie Inst Washington Yearb 65:410–414

Brophy JG, Marsh BD (1986) On the origin of high-alumina arc basalt and the mechanics of melt extraction. J Petrol 27:763–789

Carroll MR, Wyllie PJ (1989) Experimental phase relations in the system tonalite-peridotite-H_2O at 15 kbar: Implications for assimilation and differentiation processes near the crust-mantle boundary. J Petrology (in press)

Frey FA (1970) Rare earth and potassium abundances in St. Paul's Rocks. Earth Planet Sci Lett 19:37–53

Ghiorso MS (1987) Modeling magmatic systems: Thermodynamic relations. Rev Mineral 17:443–466

Ghioros MS, Carmichael ISE (1987) Modeling magmatic systems: Petrologic applications. Rev Mineral 17:467–499

Gill JB (1974) Role of underthrust oceanic crust in the genesis of a Fijiian calc-alkaline suite. Contrib Mineral Petrol 43:29–45

Grove TL, Baker MB (1984) Phase equilibrium controls on the tholeiitic vs calc-alkaline differentiation trends. J Geophys Res 89:3253–3274

Grove TL, Bryan WB (1983) Fractionation of pyroxene phyric MORB at low pressure: an experimental study. Contrib Mineral Petrol 84:293–309

Grove TL, Gerlach DC, Sando T (1982) Origin of calc-alkaline series lavas at Medicine Lake Volcano by fractionation, assimilation and mixing. Contrib Mineral Petrol 80:160–182

Hildreth W, Grove TL, Dungan MA (1986) Introduction to special section on open magmatic systems. J Geophys Res 91:5887–5889

Johnston AD (1986) Anhydrous P–T phase relations of near-primary high-alumina basalt from the South Sandwich Islands: Implications for the origin or island arc and tonalite and trondhjemite series rocks. Contrib Mineral Petrol 92:368–382

Keleman PB (1986) Assimilation of ultramafic rock in subduction-related magmatic arcs. J Geol 94:829–843

Keleman PB, Ghiorso MS (1986) Assimilation of peridotite in zoned calc-alkaline plutonic magmas: Evidence from the Big Jim complex, Washington Cascades. Contrib Mineral Petrol 94:12–28

Melson WG, Hart SR, Thompson G (1972) St. Paul's Rocks, equatorial Atlantic: Petrogenesis, radiometric ages and implications on sea-floor spreading. Geol Soc Am Mem 132:241–272

Melson WG, Jarosewich E, Bowen VT, Thompson G (1967) St. Peter's and St. Paul's rocks: A high-temperature, mantle-derived intrusion. Science 155:1532–1535

Millhollen GL, Irving AJ, Wyllie PJ (1974) Melting interval of peridotite with 5.7 percent water to 30 kbar. J Geol 82:575–587

Nehru CE, Wyllie PJ (1975) Compositions of glasses from St. Paul's peridotite partially melted at 20 kilobars. J Geol 83:455–471

Myers JD (1988) Possible petrogenetic relations between low- and high-MgO Aleutian basalts. Geol Soc Am Bull 100:1040–1053

Nicholls IA, Ringwood AE (1973) Effect of water on olivine stability in tholeiites and production of silica-saturated magmas in the island arc environment. J Geol 81:285–300

Piwinskii AJ (1968a) Studies of batholithic feldspars: Sierra Nevada, California. Contrib Mineral Petrol 17:204–223

Piwinskii AJ (1968b) Experimental studies of igneous rock series, Central Sierra Nevada Batholith, California. J Geol 76:548–570

Sekine T, Wyllie PJ (1982a) Phase relationships in the system $KAlSiO_4-Mg_2SiO_4-H_2O$ as a model for hybridization between hydrous siliceous melts and peridotite. Contrib Mineral Petrol 79:368–374

Sekine T, Wyllie PJ (1982b) Synthetic systems for modelling hybridization between hydrous siliceous magmas and peridotite in subduction zones. J Geol 90:734–741

Sekine T, Wyllie PJ (1982c) The system granite–peridotite–H_2O at 30 kbar, with applications to hybridization in subduction zone magmatism. Contrib Mineral Petrol 81:190–202

Sekine T, Wyllie PJ (1983) Experimental simulation of mantle hybridization in subduction zones. J Geol 91:511–528

Sekine T, Wyllie PJ, Baker DR (1981) Phase relationships at 30 kbar for quartz eclogite composition in $CaO-MgO-Al_2O_3-SiO_2-H_2O$ with implications for subduction zone magmas. Am Mineral 66:935–950

Stern CR, Wyllie PJ (1978) Phase compositions through crystallization intervals in basalt–andesite–H_2O at 30 kbar with implications for subduction zone magmas. Am Mineral 63:641–663

Stolper EM (1980) A phase diagram for mid-ocean ridge basalts: Preliminary results and implications for petrogenesis. Contrib Mineral Petrol 74:13–27

Takahashi E, Kushiro I (1983) Melting of a dry peridotite at high pressures and basalt magma genesis. Am Mineral 68:859–879

Volpe AM, Macdougall JD, Hawkins JW (1987) Mariana Trough basalts (MTB): Trace element ans Sr–Nd isotopic evidence for mixing between MORB-like and Arc-like melts. Earth Planet Sci Lett 82:241–254

Walker D, Shibata T, DeLong SE (1979) Abyssal tholeiites from the Oceanographer Fracture Zone, II. Phase equilibria and mixing. Contrib Mineral Petrol 70:111–125

Wyllie PJ (1979) Magmas and volatile components. Am Mineral 64:469–500

Received October 18, 1988 / Accepted March 30, 1989
Editorial responsibility: I.S.E. Carmichael